Modeling of argon–acetylene dusty plasma

Igor Denysenko, Eric von Wahl, Safa Labidi, Maxime Mikikian, Holger Kersten, Titaïna Gibert, Eva Kovacevic, Nikolay A. Azarenkov

Modelling of argon-acetylene dusty plasma

I.B. Denysenko[1], E. von Wahl[2,3], S. Labidi[3], M. Mikikian[3], H. Kersten[2],

T. Gibert[3], E. Kovačević[3] and N.A. Azarenkov[1]

[1]School of Physics and Technology, V. N. Karazin Kharkiv National University, Kharkiv, Ukraine
[2]Institut für Experimentelle und Angewandte Physik, Universität Kiel, Kiel, Germany
[3]GREMI, UMR7344 CNRS/Université d'Orléans, F-45067 Orléans, France

E-mail: idenysenko@yahoo.com

Abstract

The properties of an Ar/C_2H_2 dusty plasma (ion, electron and neutral particle densities, effective electron temperature and dust charge) in glow and afterglow regimes are studied using a volume-averaged model and the results for the glow plasma are compared with mass spectrometry measurements. It is shown that dust particles affect essentially the properties of glow and afterglow plasmas. Due to collection of electrons and ions by dust particles, the effective electron temperature, the densities of argon ions and metastable atoms are larger in the dusty glow plasma comparing with the dust-free case, while the densities of most hydrocarbon ions and acetylene molecules are smaller. Because of a larger density of metastable argon atoms and, as a result, of the enhancement of electron generation in their collisions with acetylene molecules, the electron density in the afterglow dusty plasma can have a peak in its time-dependence. The results of numerical calculations are in a good qualitative agreement with experimental results.

Keywords: argon-acetylene plasma, dust particles, glow and afterglow regimes

1. Introduction

Plasmas with nano- and micrometer-sized particles (dust particles) are of a great fundamental interest and are used in many technological applications [1-4]. The dust particles can either grow inside a discharge chamber due to different chemical reactions or can be immersed into laboratory plasmas from outside. For example, formation of carbonaceous dust particles takes place in gas discharges containing methane, acetylene or ethylene [5-7].

The plasmas used for formation of carbonaceous dust particles have been intensively investigated by experimental measurements [5-11]. The measurements in Ar/C_2H_2 plasmas showed that formation of dust particles is accompanied by a decrease of acetylene and electron densities and by an enhancement of electron temperature and density of metastable argon atoms [11-14]. It was also found that the degree of C_2H_2 dissociation in an Ar/C_2H_2 plasma at formation of nanoparticles can be as high as 99% [13, 15]. In [13], the densities of electrons and metastable argon atoms were simultaneously measured in the glow and afterglow regimes of a pulsed radio-frequency (RF) Ar/C_2H_2 plasma for the dust-free and dusty plasma cases.

Properties of C_2H_2 and Ar/C_2H_2 RF plasmas were also studied by computer simulations [16-21] allowing to explain the nucleation of nanoparticles in these chemistries. In particular, it was shown that both positive and negative ions may participate as precursors in the initial stage of particle formation [17, 19]. However, most of these numerical studies considered only the initial stages of particle formation and, therefore, they did not account for effects of dust particles on plasma properties, which may be essential in some experiments. Moreover, to the best of our knowledge, the time-dependencies for densities of ions and neutral species and the effects of dust particles in the afterglow of Ar/C_2H_2 plasmas have not been studied yet.

In this paper, the properties of an Ar/C_2H_2 dusty plasma (ion, electron and neutral particle densities, electron temperature and dust charge) in the glow and afterglow regimes are studied using a global (volume-averaged) model. The effect of dust radius on the steady-state gas-discharge properties is analysed, and the properties of dust-free and dusty-plasma afterglows are compared. The results of calculations are compared with our experimental measurements on mass spectra of positive ions and neutral species in RF dust-free and dusty plasmas.

2. Measured mass spectra of neutral species and positive ions

In our experiment, formation of dust particles took place in a capacitively coupled asymmetric discharge running in an Ar/C_2H_2 mixture. The plasma discharge was driven at 13.56 MHz and a RF power of 9 W by a RF generator coupled to the bottom electrode with the help of a matching network. The grounded electrode was the entire chamber walls. The plasma height L and radius R

were nearly 32.4 cm and 22 cm, respectively. Acetylene with the flux Q_{C2H2}=1.11 sccm and argon with the flux Q_{Ar}=10.1 sccm were used as a reactive precursor and a background gas, respectively. The process gas pressure in the reactor was about 5 Pa. The mass spectra for neutrals and positive ions were measured using the Hiden PSM 003 mass spectrometer at a height of 10 cm and a radial distance of 7 cm from the center of the powered electrode. Using this approach, we were not able to measure intensities of argon ions and neutrals at mass 40 amu simultaneously with other species because the intensity was much above saturation and the instrument would shut down.

Typical mass spectra for neutral species and positive ions, which were measured in our experiments, are shown in figures 1(*a*) and 1(*b*), respectively. The neutral mass spectrum displays that C_2H_2 (26 amu) is the dominant hydrocarbon neutral in the Ar/C_2H_2 plasma (figure 1(*a*)), while H_2 (2 amu), C_2H (25 amu), C_2H_4 (28 amu), H_2O (18 amu) and C_4H_2 (50 amu) are also significant neutral species. The peaks associated with argon atoms are observed at mass numbers 36 and 38 and additionally at 20 in the mass spectrum. The peaks associated with H (1 amu), CH (13 amu) and C_6H_2 (74 amu) are also observed. Note that the peak at mass number 28 may not be connected only with dissociation of acetylene molecules in the Ar/C_2H_2 plasma. It may be due to an input of C_2H_4 and N_2 in the discharge chamber [22]. The peaks of C_2H and CH are mainly due to C_2H_2 dissociation in the mass spectrometer. Moreover, the results for H and H_2 should be treated very carefully as the device precision is rough for very small masses.

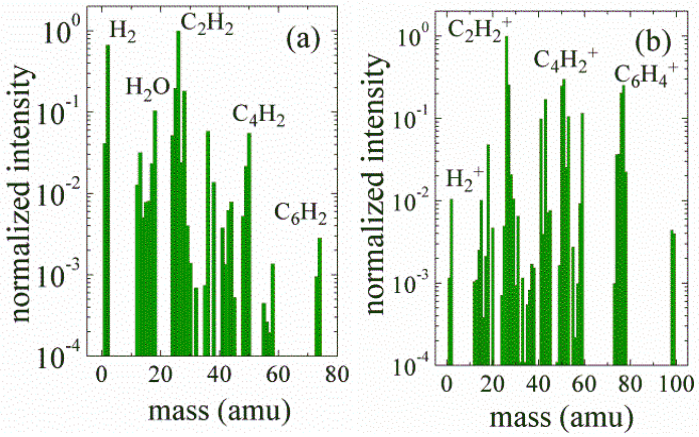

Figure 1. Mass spectra obtained in the Ar/C_2H_2 plasma for neutral species (*a*) and positive ions (*b*) for the growth phase I.

The significant ion species in the plasma are $C_2H_2^+$ (26 amu), $C_2H_3^+$ (27 amu), $C_4H_2^+$ (50 amu), $C_4H_3^+$ (51 amu), $C_6H_4^+$ (76 amu) and $C_6H_3^+$ (75 amu) (figure 1(*b*)). The ion peaks associated with ArH^+ (41 amu), H_2^+ (2 amu), and H^+ (1 amu) are about 10, 10^2 and 10^3 times smaller than the peak of $C_2H_2^+$.

After plasma ignition and under particular plasma conditions, the discharge displays a periodic behaviour. The temporal variation of, e.g. self-bias voltage V_b and the mass peaks of neutral species, is induced by the formation of carbonaceous nanoparticles. Figure 2 shows the simultaneously measured time dependency of V_b and the mass peaks of C_2H_2, H_2 and C_4H_2. Performing *ex situ* SEM measurements [23], we obtained information about the nanoparticle size in different growth phases. It was found that the measurable diameter of most dust particles is, respectively, in the range of 20 to 40 nm, 40 to 50 nm and 50 to 140 nm for the growth phases I, II and III.

Dust particles do not modify plasma properties during phase I (as V_b stays rather constant) because of their small size. This phase has to be considered carefully as it also follows phase III of the previous cycle and could be impacted by previous dust generations. During phase II, growing nanoparticles strongly disturb the plasma as seen on V_b and it corresponds to a decrease of hydrocarbon molecule signals. During phase III, these signals start increasing while nanoparticles are still growing because other dust particles possibly start to leave the discharge during phase III.

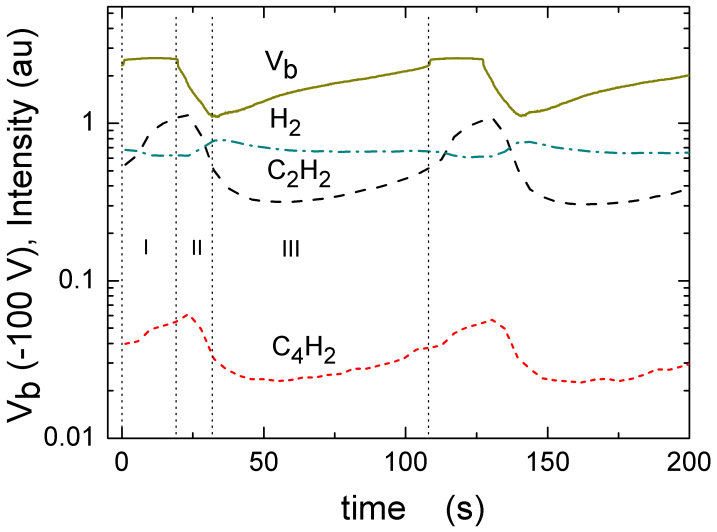

Figure 2. Time evolution of the self-bias voltage V_b and the mass peaks of C_2H_2, H_2 and C_4H_2 during a growth cycle. Here, the time t=0 corresponds to the time 2435 s from the plasma ignition.

3. The volume averaged model

The properties of the Ar/C_2H_2 dusty plasma were analysed using a volume-averaged model. In the model, the gas-discharge plasma is sustained in a cylindrical stainless steel chamber of the same dimensions as given in the above described experiment. It is assumed that the discharge consists of electrons with density n_e, nine positive ions ($C_2H_2^+$, Ar^+, ArH^+, H_2^+, H^+, $C_4H_3^+$, $C_4H_2^+$, $C_6H_4^+$ and $C_2H_3^+$), four nonradical neutrals (Ar, C_2H_2, H_2, C_4H_2) and two radicals (C_2H and H),

negatively charged dust particles with density n_d, radius a_d (in the range of 10-70 nm) and charge Z_d (in units of electron charge e), metastable argon atoms (Ar_m) with density n_m, argon atoms in the resonance 4s states ($^3P_1$ and $^1P_1$) (Ar_r) with density n_r as well as argon atoms in 4p states (Ar(4p)) with density n_{4p}. In our model, the metastable and resonance atom densities n_m, n_r and n_{4p} represent the density of a composite $^3P_0$ and $^3P_2$ metastable level, $^3P_1$ and $^1P_1$ resonance level and 4p state, respectively. We also assume that the plasma contains negative ions C_2H^- with density n^-, which is essentially larger than the densities of other anions. The latter assumption is applicable at large ratio of the argon input flux to the flux of acetylene [19-21].

It is assumed that the electron energy probability function (EEPF) F has a Druyvesteyn shape [24]. This is typical for RF plasmas with not very large electron density and sustained in large discharge chambers or at high gas pressures [25]. For example, in the case of an argon plasma driven by a RF generator of 13.56 MHz frequency, the conditions $n_e < 10^{11}$ cm^{-3} and $PL > 0.2$ Torr×cm, where P is the total gas pressure, should be fulfilled. Note that in the case when the ratio of C_2H_2 density to that of argon atoms in the power-on phase is small, the acetylene molecules do not affect much on the EEPF shape [20].

In the model, the ions and dust particles are assumed to be at gas temperature T_g (300 K). The dominant neutral species are argon atoms and their density $n_{Ar} \approx P/(k_B T_g)$, where P = 5 Pa and k_B is the Boltzmann constant.

We assume that the plasma is quasineutral, or

$$\sum_\alpha n_\alpha^+ = n_e + n^- + |Z_d| n_d , \tag{1}$$

where n_α^+ is the density of α-th positive ions.

The density of a species X (ions or neutrals) is found from the balance equation

$$\frac{\partial n^{(X)}}{\partial t} = \sum_i R_{G,i}^{(X)} - \sum_i R_{L,i}^{(X)} , \tag{2}$$

where $R_{G,i}^{(X)}$ and $R_{L,i}^{(X)}$ are, respectively, the rates for reactions describing various generation and loss processes of the species X and t is the time. In this study, we consider various processes for the loss and generation of the discharge species, including the collisional processes in the bulk plasma, the processes on plasma walls and dust particles, as well as the pumping of gas in and out of the chamber. The main electron-molecule (atom) processes taken into account in the model are presented in table 1. Their collision rates were calculated using the reaction cross sections given

in the references of table 1 and assuming that the EEPF has a Druyvesteyn shape. For the reactions of electrons with C_4H_2, the cross sections of ionization, dissociation and electron attachment are taken to be the same as those for C_2H_2, since no data are available in the literature. The cross sections describing the loss of C_2H in collisions with electrons are taken from [26]. The reactions with participation of negative ions and their rates are shown in table 2.

We also accounted for 3 reactions between hydrocarbon neutrals ($C_2H + C_2H_2 \rightarrow C_4H_2 + H$, $C_2H + C_4H_2 \rightarrow C_6H_2 + H$, $C_2H + C_4H_2 \rightarrow C_6H_2^* + H$) and for 4 reactions between H/H_2 and hydrocarbon neutral species ($H + C_2H \rightarrow C_2H_2$, $H + C_2H_2 \rightarrow C_2H_3$, $H + C_4H_2 \rightarrow C_4H_3$, $H_2 + C_2H \rightarrow C_2H_2 + H$), those reaction rates are taken from [17, 18]. The reactions for collisions of excited argon atoms with various neutral species and their rates are presented in table 3.

Table 1. Reactions for the main electron-molecule (atom) processes taken into account in the model.

Reactions between electrons and argon atoms [27-30]	
$e^- + Ar \rightarrow Ar^+ + 2e^-$	$e^- + Ar_m \rightarrow Ar(4p) + e^-$
$e^- + Ar_m \rightarrow Ar^+ + 2e^-$	$e^- + Ar_m \rightarrow Ar_r + e^-$
$e^- + Ar_r \rightarrow Ar^+ + 2e^-$	$e^- + Ar_r \rightarrow Ar_m + e^-$
$e^- + Ar(4p) \rightarrow Ar^+ + 2e^-$	$e^- + Ar_r \rightarrow Ar(4p) + e^-$
$e^- + Ar \rightarrow Ar_m + e^-$	$e^- + Ar_m \rightarrow Ar + e^-$
$e^- + Ar \rightarrow Ar_r + e^-$	$e^- + Ar_r \rightarrow Ar + e^-$
$e^- + Ar \rightarrow Ar(4p) + e^-$	$e^- + Ar(4p) \rightarrow Ar + e^-$
Reactions between electrons and hydrocarbons [26, 31]	
$e^- + C_2H_2 \rightarrow C_2H_2^+ + 2e^-$	$e^- + C_2H_2 \rightarrow C_2 + 2H + e^-$
$e^- + C_2H_2 \rightarrow H^+ + C_2H + e^-$	$e^- + C_2H_2 \rightarrow C_2H^+ + H + 2e^-$
$e^- + C_2H_2 \rightarrow C_2H^- + H$	$e^- + C_2H_2 \rightarrow C_2 + H_2 + e^-$
$e^- + C_2H_2 \rightarrow C_2H + H + e^-$	$e^- + C_2H_2 \rightarrow C_2^+ + H_2 + 2e^-$
Reactions between electrons and H/H₂ [32, 33]	
$e^- + H_2 \rightarrow 2H + e^-$	$e^- + H_2 \rightarrow H^+ + H + 2e^-$
$e^- + H_2 \rightarrow H_2^+ + 2e^-$	$e^- + H \rightarrow H^+ + 2e^-$

Table 2. Reactions with participation of negative ions.

Reaction	Rate constant (cm^3/s)	Reference
$C_2H^- + H_2^+ \rightarrow C_2H + 2H$	1.7×10^{-7}	[17]
$C_2H^- + H^+ \rightarrow C_2H + H$	3.0×10^{-8}	[18]
$C_2H^- + ArH^+ \rightarrow C_2H + H + Ar$	3.0×10^{-8}	
$C_2H^- + C_2H_2 \rightarrow C_4H^- + H_2$	1.0×10^{-12}	[18]
$C_2H^- + C_mH_n^+ \rightarrow C_2H + C_mH_n$	5.0×10^{-8}	[18]
$C_2H^- + Ar^+ \rightarrow C_2H + Ar$	1.01×10^{-7}	[20]
$C_2H^- + H \rightarrow C_2H_2 + e^-$	1.6×10^{-9}	[34]

It is also accounted for 6 reactions between Ar^+/ArH^+ and neutral species [20, 35, 36], 29 reactions between hydrocarbon ions and neutral species [18, 37-44] and 7 reactions between H_2^+/H^+ and neutrals [18, 36, 37, 40].

The rates describing the pumping gas in and out of the chamber were calculated in the same way as in [45]. The rate describing the radical loss due to diffusion to the walls is taken as in [46, 47]. For the radical neutrals and excited argon atoms, it is also accounted for their deposition on dust particles. The sticking coefficients for C_2H, H and excited argon atoms are assumed to be 0.9, 0.1 and 1.0, respectively [17, 48, 49]. The amount of hydrogen incorporated into the walls and dust particles due to their interaction with C_2H and H radical neutrals is set to 30%, the other amount of atomic hydrogen flows back into the plasma as molecular hydrogen gas [50]. The rates describing the positive ion loss on dust particles are calculated using the orbit-motion-limited theory [1], accounting for the ion-neutral collisions in the sheath of the dust particle [51]. We do not account for negative ion loss on dust particles and the walls because their energy is assumed to be essentially smaller than the potentials of the walls and the dust surface.

Table 3. Reactions with participation of argon atoms in excited states. Here, Ar* denotes argon atoms in various excited states including the metastable and 4s and 4p resonance states.

Reaction	Rate constant (cm^3/s)	Reference
$Ar^* + C_2H_2 \rightarrow C_2H_2^+ + Ar + e^-$	1.8×10^{-10}	
$Ar^* + C_2H_2 \rightarrow C_2H + Ar + H$	3.5×10^{-10}	
$Ar^* + C_4H_2 \rightarrow C_4H_2^+ + Ar + e^-$	1.8×10^{-10}	
$Ar^* + C_4H_2 \rightarrow C_4H + Ar + H$	3.5×10^{-10}	
$Ar^* + H_2 \rightarrow ArH^* + H$	1.1×10^{-10}	[35]
$Ar_m + Ar_m \rightarrow Ar + Ar^+ + e^-$	6.2×10^{-10}	[52]
$Ar_m + Ar_m \rightarrow 2Ar$	2.0×10^{-7}	[37]
$Ar_m + Ar_r \rightarrow Ar + Ar^+ + e^-$	2.1×10^{-9}	[37]
$Ar(4p) + Ar(4p) \rightarrow Ar^+ + Ar + e^-$	5.0×10^{-10}	[37]
$Ar_m + Ar \rightarrow 2Ar$	2.1×10^{-15}	[37]
$Ar_r \rightarrow Ar + \hbar\omega$	$10^5\ s^{-1}$	[37]
$Ar(4p) \rightarrow Ar + \hbar\omega$	$3.2\times10^7\ s^{-1}$	[37]
$Ar(4p) \rightarrow Ar_m + \hbar\omega$	$3.0\times10^7\ s^{-1}$	[37]
$Ar(4p) \rightarrow Ar_r + \hbar\omega$	$3.0\times10^7\ s^{-1}$	[37]

The ion mobility and ion diffusion coefficients were calculated in the same manner as in [53], while the expression for the rate describing the loss of a positive ion on the walls is taken from [46].

The next equation of our model for the steady-state case is the power balance equation

$$P_{abs} = P_{coll} + P_w + P_d, \tag{3}$$

where P_{abs} is the absorbed power (in the experiment, $P_{abs} = 9$ W), P_{coll} and P_w are the power loss due to elastic and inelastic collisions and the loss due to charged particle fluxes to the walls, respectively [46]. P_d is the power loss on the dust [54]. In calculating the power loss in collisional

processes, we accounted for the loss in collisions of electrons with C_2H_2, C_4H_2, H_2 and Ar with cross sections from [55-58].

The dust charge Z_d is obtained from the following equation

$$\frac{\partial |Z_d|}{\partial t} = K_d^e n_e - \sum_\alpha K_d^\alpha n_\alpha^+, \tag{4}$$

where the rates K_d^e and K_d^α describe, respectively, collection of electrons and positive ions of sort α by dust particles. The expressions for these rates can be found elsewhere [52, 59].

Considering the afterglow case, we assume that the effective electron temperature decays exponentially according to $T_e(t) = T_{e0} \exp(-t/\tau_T)$ with the decay time τ_T=50 μs, like in [52] and T_{e0} the temperature in the power-on phase. We also assume that due to the production of energetic electrons in metastable–metastable collisions, super-elastic electron–metastable collisions and emission processes, the electron temperature cannot be smaller than 0.1 eV, i.e. after its decay to reach 0.1 eV, T_e becomes time-independent.

For the steady-state case, the balance equations for C_2H_2, H_2 and H and equation (3) were solved by the iteration method (assuming $d/dt = 0$) simultaneously with the balance equations for other species and equation (4), which were solved by the 4-th order Runge-Kutta method. Applying the Runge-Kutta method, the system of first order differential equations was allowed to reach a steady state, i.e. $d/dt = 0$.

For the afterglow case, the balance equations for different species and dust charge were solved by the 4-th order Runge-Kutta method, using the initial values obtained in the steady-state calculations.

4. The results of calculations

4.1 Effects of variation of dust radius on the steady-state plasma properties

Using the theoretical model presented in section 3, we have analysed how dust particles affect the densities of various ions and neutral species in the Ar/C_2H_2 glow plasma. In our calculations, we varied a_d, while other external parameters including n_d, were fixed.

For the glow plasma, we assumed that the plasma is stationary because the density variation of various species due to dust growth [9, 23] is usually longer than the variations due to various collisional processes and diffusion to the walls.

The dust charge magnitude increases with increasing a_d because of the increase of the dust surface collecting electrons and because of the increase of T_e, while n_e decreases [60]. For a_d = 10,

20, 40, 60 nm, n_e =1.82×10^9, 1.25×10^9, 4.34×10^8 and 1.76×10^8 cm^{-3} and Z_d = -36, -68, -113 and -130 respectively, for the conditions of figure 3. In figure 3, the calculated densities of neutral species and ions as functions of dust radius are shown. One can see in figure 3(a) that C_2H_2 and H_2 are the dominant molecules in the gas discharge, in agreement with our experimental measurements (figure 1(a)).

For the dust-free case (a_d=0), the argon atom density ($n_{Ar} \approx 1.21\times10^{15}$ cm^{-3} for P ~ 5 Pa) is 453 times larger than the density of C_2H_2 ($n_{C2H2} \approx 2.67\times10^{12}$ cm^{-3}) and the degree of dissociation of C_2H_2 in the plasma is nearly 98 %. This agrees well with the degree estimations in [15] showing that it is in the range of 95%-99% at formation of nanoparticles.

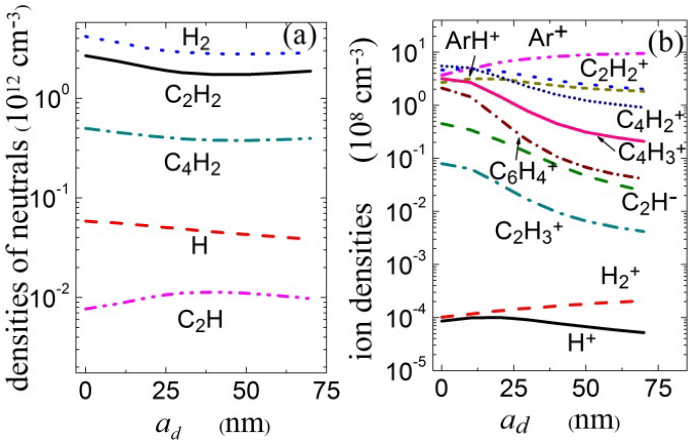

Figure 3. Calculated densities of neutral species (a) and ions (b) as functions of dust radius. The results are obtained for P_{abs} = 9 W, n_d =10^7 cm^{-3}, Q_{C2H2} =1.11 sccm and Q_{Ar} = 10.1 sccm.

The loss of C_2H_2 molecules in the plasma is mainly due to their collisions with metastable atoms, positive ions, C_2H radicals and electrons. For the case of small particles ($a_d \leq 40$ nm) the density of acetylene molecules decreases with growing particle radius (figure 3(a)) as this is accompanied by an increase of the densities of argon ions and metastable atoms, C_2H radicals and by an increase of the effective electron temperature. For the case of bigger particles ($a_d \geq 50$ nm), however, the C_2H_2 density slightly increases with an increase of a_d because of the n_e reduction. The C_4H_2 and H_2 production is related to the C_2H_2 density [11], and, as a result, the a_d - dependencies for the C_4H_2 and H_2 densities are similar to that for n_{C2H2}. The decrease of H density at larger dust radius is due to higher losses of hydrogen atoms on dust particles and to a decrease of the densities of nonradical molecules and electrons, whose collisions affect the radical production. Since the main production process of C_2H are the collisions of excited argon atoms with acetylene molecules and C_2H is predominantly lost in the collisions with C_2H_2, the dependence of C_2H on a_d is determined mainly by the a_d-dependencies for densities of excited argon atoms (n_m is presented in figure 4) and acetylene molecules (figure 3).

The results of calculations are in a good qualitative agreement with the experimental results revealing that the densities of C_2H_2 and C_4H_2 are decreasing with increasing the time (the dust radius) during phase II and the beginning of phase III (figure 2). However, there is a discrepancy between the simulation results and experimental data. In particular, the measured density of H_2 is smaller than the one of acetylene molecules during phases I and II while it's always larger in the model. The discrepancy may be due to the simplifications introduced in the 0D model. For example, our global model does not account for the spatial inhomogeneity of the plasma, while the spatial distributions of ions, radicals and dust particles are usually essentially inhomogeneous in Ar/C_2H_2, C_2H_2 and dusty plasmas [17, 20, 61]. We also do not account for the variation of neutral gas temperature during the growth cycle [62].

The dominant ions in the dust-free plasma are Ar^+, $C_2H_2^+$, $C_4H_2^+$, $C_4H_3^+$, $C_6H_4^+$ and ArH^+. This agrees well with our measurements of mass spectrum for positive ions (figure 1(b)). The concentrations of H_2^+ and H^+ are essentially smaller than those of the dominant ions because of their intensive loss in the collisions with argon atoms and acetylene molecules, respectively. It is also due to the fact that the cross-section for ionization of C_2H_2 by electrons is larger than those for H_2 and H [17].

The densities of Ar^+ and H_2^+ increase with enlarging particles (a_d), while the densities of other ions including $C_2H_2^+$ are decreasing. These variations are mainly caused by the decrease of the electron density and the increase of the effective electron temperature (figure 4).

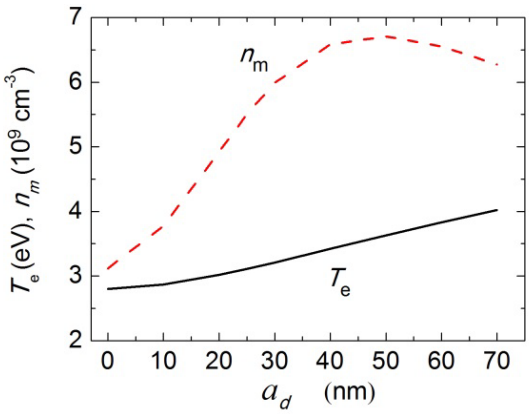

Figure 4. n_m and T_e as functions of dust radius. The conditions are the same as in figure 3.

As ground-state Ar atoms have a larger ionization threshold energy than C_2H_2 molecules, the increase of T_e favours Ar^+ production. Therefore, the H_2^+ density increase is mainly due to the enhancement of H_2^+ production in collisions of Ar^+ with H_2. Since the dominant production processes of $C_4H_2^+$ and $C_4H_3^+$ are the collisions of $C_2H_2^+$ with C_2H_2, the decrease of the acetylene density with a_d leads to a reduction of the density of these ions.

For the same reasons, the $C_2H_3^+$ production, mainly due to $C_2H_2^+$ - H_2 collisions, decreases with a_d. The $C_6H_4^+$ density reduces also with a_d because of the decrease of $C_4H_2^+$ and C_2H_2 densities ($C_6H_4^+$ is produced by collisions between $C_4H_2^+$ and C_2H_2) and due to higher losses of $C_6H_4^+$ on dust particles. The smaller ArH^+ density at larger a_d is mainly due to the enhancement of the ion loss on the dust.

The metastable atom density increases with a particle enlargement from $a_d = 0$ to $a_d = 50$ nm and then decreases at larger dust radii. This is caused by an enlargement of T_e and by the n_e decrease, respectively (figure 4).

The concentration of negative ions C_2H^- decreases with growing particle radius due to a reduction of the anion generation by the attachment of electrons to C_2H_2 (since n_e decreases), as well as due to an enhancement of the negative ion loss in collisions with Ar^+ ions.

4.2 The afterglow of C_2H_2 plasma

In this subsection, we will analyze how dust particles affect the C_2H_2 plasma afterglow. In figure 5, the densities of C_2H and H radicals are shown during dust-free and dusty-plasma afterglows. The density of C_2H decreases more rapidly with time t in the dust-free afterglow comparing with the dusty case. This is due to larger C_2H_2 density in the dust-free case (figure 3(a)) and, as a result, more intensive loss of C_2H in collisions with C_2H_2 ($C_2H + C_2H_2 \rightarrow C_2H_2 + H$). The decay time for H in dust-free plasma afterglow is nearly the same as that in dusty plasma case because the loss of H in both cases is mainly defined by the diffusion to the walls. In the dusty case, the loss of H on dust particles for small dust radius and density, considered here, is small.

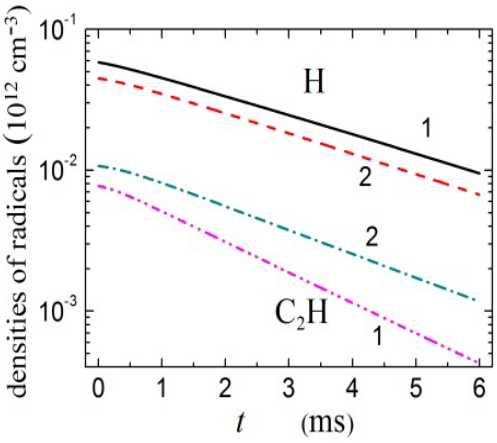

Figure 5. Calculated densities of C_2H and H in the dust-free (curves 1) and dusty-plasma (curves 2) afterglows as functions of time. The results are obtained for a_d=25 nm, $n_d = 10^7$ cm^{-3}. The other external conditions are the same as in figure 3.

The decay times for radical species (H and C_2H) are small because the frequencies

characterizing the radical losses (due to the diffusion to the walls and their collisions with nonradical neutrals) are rather large. For example, the frequency characterizing the loss of C_2H in collisions with C_2H_2 for $n_{C2H2} = 2\times10^{12}$ cm^{-3} is 2.6×10^2 s^{-1}, i.e. the decay time is about 4 ms.

In the afterglow, the densities of radical species, ions, metastable argon atoms and electrons are decreasing with time (figures 5 - 7), and, as a result, the density of C_2H_2 is increasing because of acetylene injection into the discharge chamber, while the densities of H_2 and C_4H_2 become smaller because of less intensive generation of these molecules from C_2H_2. The time $t_1 = R/n_{C2H2}(0)$, characterizing the C_2H_2 density increase in the afterglow is about 0.5 s. Here, it was used: $R = 4.48\times10^{17} Q_{C2H2}/V$, Q_{C2H2}=1.11 sccm, V the plasma volume and $n_{C2H2}(0) = 2\times10^{12}$ cm^{-3} the acetylene density in the power on phase.

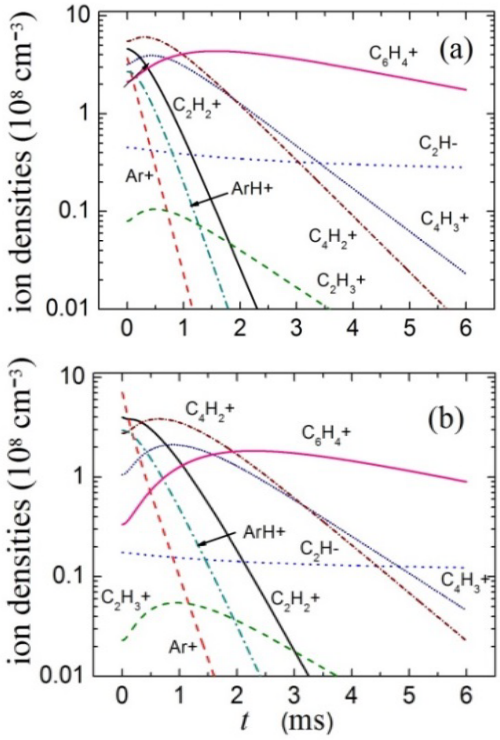

Figure 6. Calculated densities of main ions in the dust-free (a) and dusty-plasma (b) afterglows as functions of time. The conditions are the same as in figure 5.

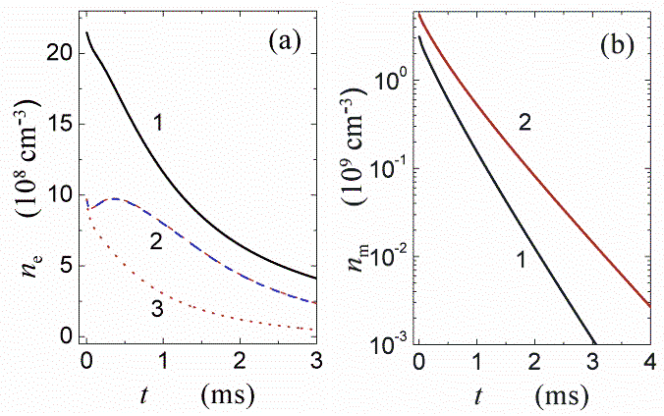

Figure 7. (a) n_e as a function of time for the dust-free case (curve 1) and for the dusty-plasma cases when the electron generation in Ar_m- C_2H_2 collisions is taken into account (curve 2) and neglected (curve 3). (b) The density of Ar_m for the dust-free (curve 1) and dusty-plasma (curve 2) cases accounting for all the collisional processes. The external conditions are the same as in figure 5.

The times characterizing losses of nonradical species, C_2H_2, H_2 and C_4H_2, in which are caused by collisions with radical species, ions, metastable argon atoms and electrons are essentially larger than for radical neutrals because of small frequencies for these collisions. For example, the frequencies and corresponding times characterizing the loss of C_2H_2 in collisions with C_2H, Ar^+ and Ar_m for $n_{C2H} = 10^{10}$ cm^{-3}, $n_{Ar^+} = 10^9$ cm^{-3}, $n_m = 5\times10^9$ cm^{-3} are, respectively, 1.3, 0.42 and 2.65 s^{-1}; 0.77, 2.38 and 0.38 s.

Thus, the densities of nonradical species, C_2H_2, H_2 and C_4H_2, are nearly independent on time for the afterglow times considered here. The long time scales for feeding new C_2H_2 molecules and for losses of C_2H_2, H_2 and C_4H_2 explain this stability in the ms range.

The densities of $C_2H_2^+$, Ar^+ and ArH^+ decrease during the afterglow due to a reduction of the effective electron temperature, n_e and n_m (figure 7). Their main loss mechanism are the collisions with nonradical neutrals, which are having a relatively constant density in the ms time scale. And therefore, the ion losses do not change much in the afterglow. The decay time for Ar^+ is smaller than that for other ions because it exclusively produced in electron-neutral collisions, while other ions are also produced in collisions of neutrals with ions and/or metastable atoms.

Diffusion to the walls is one of the main loss processes for $C_2H_3^+$, $C_4H_2^+$, $C_4H_3^+$ and $C_6H_4^+$, and it is strongly reduced in the afterglow because of the decrease of T_e. They are predominantly produced in collisions of ions and metastable argon atoms with neutrals. In the beginning of the afterglow, the production dominates over the losses by diffusion, and, therefore, the ion densities increase.

Note also that at large afterglow times ($t > 2$ ms), the density of $C_6H_4^+$ decreases more slowly than for other ions because of the smaller rate of collision with C_2H_2 (7×10^{-11} cm^3/s) compared to other ions (for example, 1.2×10^{-9} cm^3/s for $C_2H_2^+$- C_2H_2 collisions). Moreover, the decay time due to diffusion to the walls increases with increasing the ion mass due to lower velocities. The

densities of Ar^+, $C_2H_2^+$, ArH^+, $C_2H_3^+$, $C_4H_2^+$ and $C_4H_3^+$ ions decrease faster in the dust-free case than in the dusty one. In our opinion, this is due to larger densities of C_2H_2 and H_2 in the former case and, as a result, more intensive loss of these ions in collisions with the molecules.

The density of negative ions decreases more slowly than the one of positive ions. This is due to the model assumption that the anions do not deposit on the plasma walls and to a smaller collision rate with C_2H_2 for C_2H^- than for positive ions. The decrease of the anion density at large afterglow times is mainly due to the collisions with hydrogen atoms.

We have also analyzed the time-dependence for n_e in the dust-free and dusty plasma afterglows. One can see in figure 7 that the density of electrons in the dust-free case decreases during the whole afterglow time (curve 1). This is mainly due to electron diffusion to the walls. In the dusty case, the electron density drops at very small afterglow times (t < 0.05 ms) and then increases at 0.05 ms < t < 0.35 ms (curve 2).

The time-dependencies for electron density in the dust-free and dusty afterglows are similar to those obtained for argon plasma afterglows [52]. The presence of a peak in the time-dependence for n_e in the case of argon dusty afterglow was explained by the release of free electrons from the dust particles [10] and/or by the electron generation in metastable-metastable collisions [52]. Here, in the Ar/ C_2H_2 case, we find, that the electron production in collisions of metastable atoms with acetylene molecules ($Ar_m + C_2H_2 \rightarrow C_2H_2^+ + Ar + e^-$) [13] is responsible for it. To check the latter conclusion, the calculations were carried out without this process leading to curve 3 in figure 7 without any peak. We also carried out the calculations neglecting the electron generation in metastable-metastable collisions, and the effect of this process on the time-dependence of n_e was found to be small.

The metastable density is larger in the dusty-plasma afterglow than that in the dust-free case (figure 7(b)) because of larger effective electron temperature at t =0 in the former case. n_m decreases more slowly in the dusty-plasma afterglow because the metastable losses are mainly due to their collisions with C_2H_2, H_2 and C_4H_2 (the densities of these molecules are larger in the dust-free case). Due to the losses in collisions with neutrals, the metastable density decreases more rapidly in the Ar-C_2H_2 plasma afterglow than in the Ar one (please, compare the curves in figure 7 of this paper with the curves in figure 6(a) of [52]), in agreement with experimental results of Stefanovic et al. (figure 8 of [13]).

The dust charge as a function of time in the afterglow was also calculated. It was found that the dependence for Z_d is similar to that in argon dusty afterglow (figure 4(c) in [52]). For the conditions corresponding to curve 2 in figure 7(a), the dust charge at t = 3 ms was found to be -5e. Note that the dust charge fluctuation due to the discreteness of the charging process is rather large here [63-65]. In this case, the deviation from the equilibrium dust charge δZ_d

($\approx|Z_d|^{1/2}\sqrt{(\tau+z)/z(1+\tau+z)}$ [63], where $\tau = T_i/T_e$, T_i is the ion temperature and $z=e^2|Z_d|/a_dT_e$ or $\delta Z_d \approx 0.5|Z_d|^{1/2}$ [64]) is nearly 1.1. Thus, $\delta Z_d/Z_d \approx 0.22$ for the case considered here. The deviation is smaller in the glow case and increases with increasing the afterglow time and decreasing a_d. Therefore, our approach for description of dust charge is approximate for large afterglow times and nanometre-sized particles. Meantime, in [66], it was shown that the time-dependence for electron density in a dusty plasma afterglow calculated using the orbital motion limited theory agrees well with that obtained using the Monte Carlo approach. Note also that our approach for calculation of Z_d does not account for a release of electrons from dust particles by ion bombardment due to field induced emission or by other mechanisms [66]. If the electron emission yield is of the order of 1, the electron release from dust particles may essentially affect plasma properties [52, 66]. Meantime, experiments show that the value of the intrinsic secondary electron yield from carbonaceous dust material is essentially smaller than 1 [66]. Our model for dust charging also assumes that the dust particles are spherical. However, in some experiments the shape of dust particles may be not spherical affecting essentially the collection of electrons and ions by dust particles and the particle motion in the plasma [67, 68].

Therefore, the dust charging model here may be used only for qualitative analysis of the dust charging process in Ar/C_2H_2 plasmas. For quantitative analysis of the problem, one has to account in the model for the charge discreteness, different secondary emission processes and for nonsphericity of dust particles.

5. Summary

In summary, we have analysed by a spatially-averaged model how dust particles affect the properties of glow and afterglow Ar/C_2H_2 plasmas. For the glow plasma case, it has been shown that the densities of C_2H_2, H_2 and C_4H_2 molecules at the same external conditions are smaller in the dusty plasma than in the dust-free case due to the enhancement of their losses in various collisional processes. This enhancement is mainly due to the increase of the effective electron temperature caused by collection of electrons on the dust. The temperature increase is accompanied by more intensive production of Ar^+ ions and, as a result, by an increase of their density. Meantime, due to enhanced collection of electrons and ions by dust particles, the densities of most hydrocarbon ions reduced at bigger dust radius. Because of the competition between the increase of T_e and the decreasing of n_e, the metastable atom density grows with a_d at moderate dust radii (here, $a_d \leq 50$ nm) and decreases at larger dust radii. The dust particles also affect the radical, ion and electron concentrations and the density of metastable argon atoms in the Ar/C_2H_2 plasma afterglow. Since the density of acetylene molecules is larger in a dust-free plasma than in the dusty one, the densities of C_2H radicals, most positive ions and metastable argon atoms

decrease more rapidly in the afterglow as a consequence of their intensified losses in collisions with nonradical neutrals. Due to the larger density of argon metastable atoms in the dusty plasma in turn, the electron production from collisions between metastable atoms and C_2H_2 molecules is more intensive leading to a possible peak in the electron density during the afterglow. The model and numerical results presented here are different from those proposed in our earlier studies and the works of previous authors. In particular, our previous numerical results on glow and afterglow dusty plasmas [52, 54] were obtained neglecting chemical processes in plasma volume. While in the earlier works on Ar/C_2H_2 and C_2H_2 plasmas [16–21] the effects of dust particles on the plasmas have not been considered. The numerical results for glow and afterglow regimes presented here are obtained accounting for main chemical processes in Ar/C_2H_2 plasma, as well as the effects of dust particles on plasma properties. The results for the glow regime are compared and found to be in a good qualitative agreement with our recent experimental results on glow Ar/C_2H_2 plasma, while the numerical results on the afterglow plasma are in a good qualitative agreement with experimental results from the literature. The presented results are relevant to many applications involving chemically-active plasmas containing impurities, especially gas discharge plasmas used for the synthesis of novel nanomaterials.

Acknowledgements

One of the authors (I. B. D.) was supported by the Humboldt Foundation. S.L., T.G. and M.M. were supported by the CNRS through PICS n°07368 and by the PHC PROCOPE project n°30790RL from Ministères des Affaires Etrangères et du Développement International (MAEDI) et de l'Education Nationale de l'Enseignement Supérieur et de la Recherche (MENESR). E. v. W. was supported in the frame of the SFB TR24 in the project B13.

References

References

[1] *Dusty Plasmas: Physics, Chemistry, and Technological Impacts in Plasma Processing*, edited by A. Bouchoule A 1999 (New York: Wiley)

[2] Vladimirov S V and Ostrikov K 2004 *Phys. Rep.* **393** 175

[3] Winter J 2004 *Plasma Phys. Control. Fusion* **46** B583

[4] Mikikian M, Labidi S, von Wahl E, Lagrange J F, Lecas T, Massereau-Guilbaud V, Géraud-Grenier I, Kovacevic E, Berndt J, Kersten H and Gibert T 2017 *Plasma Phys. Control. Fusion* **59** 014034

[5] Hong S, Berndt J and Winter J 2003 *Plasma Sources Sci. Technol*. **12** 46

[6] Deschenaux Ch, Affolter A, Magni D, Hollenstein Ch and Fayet P 1999 *J. Phys. D: Appl. Phys*. **32** 1876

[7] Benedikt J, Consoli A, Schulze M and von Keudell A 2007 *J. Phys. Chem. A* **111** 10453

[8] Thejaswini H C, Peglow S, Martens U, Sushkov V and Hippler R 2014 *Contrib. Plasma Phys.* **54** 683

[9] Do H T, Thieme G, Frohlich M, Kersten H and Hippler R 2005 *Contrib. Plasma Phys*. **45** 378

[10] Winter J, Berndt J, Hong S H, Kovačević E, Stefanović I and Stepanović O 2009 *Plasma Sources Sci. Technol.* **18** 034010

[11] Herrendorf A P, Sushkov V and Hippler R 2017 *J. Appl. Phys*. **121** 123303

[12] Berndt J, Kovacevic E, Stefanovic I and Boufendi L 2009 *J. Appl. Phys.* **106** 063309

[13] Stefanović I, Sadeghi N, Winter J and Sikimić B 2017 *Plasma Sources Sci. Technol*. **26** 065014

[14] Winter J, Berndt J, Hong S H, Kovačević E, Stefanović I and Stepanović O 2009 *Plasma Sources Sci. Technol.* **18**034010

[15] Stefanović I, Sadeghi N and Winter J 2010 *J. Phys. D: Appl. Phys.***43** 152003

[16] Stoykov S, Eggs C and Kortshagen U 2001 *J. Phys. D: Appl. Phys*. **34** 2160

[17] De Bleecker K, Bogaerts A and Goedheer W 2006 *Phys. Rev. E* **73** 026406

[18] Mao M, Benedikt J, Consoli A and Bogaerts A 2008 *J. Phys. D: Appl. Phys*. **41** 225201

[19] Ariskin D A, Schweigert I V, Alexandrov A L, Bogaerts A and Peeters F M 2009 *J. Appl. Phys.* **105** 063305

[20] Schweigert I V, Alexandrov A L and Ariskin D A 2014 *Plasma Chem. Plasma Process*. **34** 671

[21] Akhoundi A and Foroutan G 2017 *Phys Plasmas* **24** 053516

[22] Consoli A, Benedikt J and von Keudell A 2008 *J. Phys. Chem. A* **112** 11319

[23] Hinz A M, von Wahl E, Faupel F, Strunskus T and Kersten H 2015 *J. Phys. D: Appl. Phys*. **48** 055203

[24] Gudmundsson J T 2001 *Plasma Sources Sci. Technol.* **10** 76

[25] Godyak V A, Piejak R B and Alexandrovich B M 1992 *Plasma Sources Sci. Technol*. **1** 36

[26] Janev R K and Reiter D 2004 *Phys. Plasmas*. **11** 780

[27] Yanguas-Gil A, Cotrino J and Alves L 2005 *J. Phys. D: Appl. Phys*. **38** 1588

[28] Ali M A and Stone P M 2008 *Int. J. Mass Spectrom*. **271** 51

[29] Deutsch H, Becker K, Grum-Grzhimailo A N, Bartschat K, Summers H, Probst M, Matt-Leubner S and Märk T D 2004 *Int. J. Mass Spectrom*. **233** 39

[30] Mityureva A A and Smirnov V V 2004 *Opt. Spektrosk*. **97** 508

[31] Rutrowsky J, Drost H and Spangenber H J 1980 *Ann. Phys*. **492** 259

[32] Shah M B, Elliott D S and Gilbody H B 1987 *J. Phys. B: At. Mol. Phys*. **20** 3501

[33] Yoon J S, Song M Y, Han J M, Hwang S H, ChangW S, Lee B J and Itikawa Y 2008 *J. Phys. Chem. Ref. Data* **37** 913

[34] Barckholtz C, Snow T P and Bierbaum V M 2001 *Astrophys. J*. **547** L171

[35] Gordillo-Vazquez F J and Albella J M 2003 *J. Appl. Phys.* **94** 6085

[36] Sode M, Jacob W, Schwarz-Selinger T and Kersten H 2015 *J. Appl. Phys*. **117** 083303

[37] Hjartarson A T, Thorsteinsson E G and Gudmundsson J T 2010 *Plasma Sources Sci. Technol*. **19** 065008

[38] Knight J S, Freeman C G, McEwan M J, Anicich V G and Huntress Jr W T 1987 *J. Phys. Chem.* **91** 3898

[39] Anicich V and McEwan M 1997 *Planet. Space Sci*. **45** 897

[40] http://www.udfa.net/

[41] Herbst E and Leung C 1989 *Ap. J. Supl. Ser*. **69** 271

[42] Moses J I and Bass S F 2000 *J. Geophys. Res*. **105** 7013

[43] Miasek P G and Beauchamp J L 1979 *In. J. Mass Spectrom. Ion Phys*. **15** 49

[44] McEwan M J, Scott G B I, Adams N G, Babcock L M, Terzieva R and Herbst E 1999 *Astrophys. J.* **513** 287

[45] Denysenko I B, Xu S, Long J D, Rutkevych P P, Azarenkov N A and Ostrikov K 2004 *J. Appl. Phys*. **95** 2713

[46] Thorsteinsson E G and Gudmundsson J T 2009 *Plasma Sources Sci. Technol*. 18 045001

[47] Booth J P and Sadeghi N 1991 *J. Appl. Phys.* **70** 611

[48] Sode M, Schwarz-Selinger T, Jacob W and Kersten H 2014 *J. Appl. Phys.* **116** 013302

[49] Cvelbar U, Mozetič M, Poberaj I, Babič D and Ricard A 2005 *Thin Solid Films* **475** 12

[50] Herrebout D, Bogaerts A, Yan M, Gijbels R, Goedheer W and Dekempeneer E 2001 *J. Appl. Phys.* 90 570

[51] Khrapak S A, Ratynskaia S V, Zobnin A V, Usachev A D, Yaroshenko V V, Thoma M H, Kretschmer M, Hofner H, Morfill G E, Petrov O F and Fortov V E 2005 *Phys. Rev. E* **72** 016406

[52] Denysenko I, Stefanović I, Sikimić B, Winter J, Azarenkov N A and Sadeghi N A 2011 *J. Phys. D: Appl. Phys*. **44** 205

[53] Mcdaniel E W and Mason E A 1973 *The mobility and diffusion of ions in gases* (New York: John Wiley & Sons)

[54] Denysenko I, Yu M Y, Ostrikov K and A. Smolyakov A 2004 *Phys. Rev. E* **70** 046403

[55] Phelps A V and Petrovic Z Lj 1999 *Plasma Sources Sci. Technol*. **8** R21

[56] Hayashi M 1990 Electron collision cross sections determined from beam and swarm data by Boltzmann analysis *Nonequilibrium Processes in Partially Ionized Gases* ed M Capitelli and J N Bardsley (New York: Plenum)

[57] Morgan database, www.lxcat.net

[58] Fite W L and Brackmann R T 1958 *Phys. Rev.* **112** 1151

[59] Denysenko I B, Kersten H and Azarenkov N A 2015 *Phys. Rev. E* **92** 033102

[60] Wegner Th, Hinz A M, Faupel F, Strunskus T, Kersten H and Meichsner J 2016 *Appl. Phys. Lett.* **108** 063108

[61] Mikikian M, Boufendi L, Bouchoule A, Thomas H M, Morfill G E, Nefedov A P, Fortov V E and the PKE-Nefedov Team 2003 *New J. Phys*. **5** 19

[62] Sushkov V, Herrendorf A P and Hippler R 2016 *J. Phys. D: Appl. Phys.* **49** 425201

[63] Morfill G E, Tsytovich V N and Thomas H 2003 *Plasma Phys. Rep.* **29** 1

[64] Cui C and Goree J 1994 *IEEE Trans. Plasma Sci*. **22** 151

[65] Piel A and Melzer A 2002 *Plasma Phys. Control. Fusion* **44** R1

[66] Stefanović I, Berndt J, Marić D, Šamara V, Radmilović-Radjenović M, Petrović Z Lj, Kovačević E and Winter J 2006 *Phys. Rev. E* **74** 024606

[67] Miloch W J, Vladimirov S V, Pécseli H L and Trulsen J 2008 *Phys. Rev. E* **78** 036411

[68] Mahmoodi J, Shukla P K, Tsintsadze N L and Tskhakaya D D 2000 *Phys. Rev. Lett*. **84** 2626